



Cite this: *Analyst*, 2015, **140**, 4828

Fine tuning of nanopipettes using atomic layer deposition for single molecule sensing†

Jasmine Y. Y. Sze,^a Shailabh Kumar,^{b,c} Aleksandar P. Ivanov,^a Sang-Hyun Oh^{b,c} and Joshua B. Edel^{*a}

Nanopipettes are an attractive single-molecule tool for identification and characterisation of nucleic acids and proteins in solutions. They enable label-free analysis and reveal individual molecular properties, which are generally masked by ensemble averaging. Having control over the pore dimensions is vital to ensure that the dimensions of the molecules being probed match those of the pore for optimization of the signal to noise. Although nanopipettes are simple and easy to fabricate, challenges exist, especially when compared to more conventional solid-state analogues. For example, a sub-20 nm pore diameter can be difficult to fabricate and the batch-to-batch reproducibility is often poor. To improve on this limitation, atomic layer deposition (ALD) is used to deposit ultrathin layers of alumina (Al₂O₃) on the surface of the quartz nanopipettes enabling sub-nm tuning of the pore dimensions. Here, Al₂O₃ with a thickness of 8, 14 and 17 nm was deposited onto pipettes with a starting pore diameter of 75 ± 5 nm whilst a second batch had 5 and 8 nm Al₂O₃ deposited with a starting pore diameter of 25 ± 3 nm respectively. This highly conformal process coats both the inner and outer surfaces of pipettes and resulted in the fabrication of pore diameters as low as 7.5 nm. We show that Al₂O₃ modified pores do not interfere with the sensing ability of the nanopipettes and can be used for high signal-to-noise DNA detection. ALD provides a quick and efficient (batch processing) for fine-tuning nanopipettes for a broad range of applications including the detection of small biomolecules like RNA, aptamers and DNA–protein interactions at the single molecule level.

Received 18th May 2015,

Accepted 3rd June 2015

DOI: 10.1039/c5an01001b

www.rsc.org/analyst

Introduction

Single-molecule detection in biomedical and biotechnological applications provides the opportunity to study individual molecules and identify rare events usually masked by ensemble averaging. One powerful technique to perform such studies in label-free conditions is nanopore sensing. In nanopore sensing^{1–3} individual biological analytes are translocated through a nanoscale pore in a thin insulating membrane and are identified by characteristic modulations in the nanopore current. Solid-state nanopores can be fabricated from various materials including SiN_x,^{4–6} SiO₂,^{7,8} graphene^{9,10} amongst others.^{11,12} A sub-class of solid-state nanopores, nanopipettes, are typically made from quartz or borosilicate glass and provide some advantages such as quick, low-cost fabrication,¹³

low-noise performance,^{14,15} chemical stability,^{16,17} easier handling, high-aspect ratio geometry and simple routes for multiplexed sensing.¹⁸ Due to these advantages, the use of nanopipettes has steadily increased in the detection of DNA,^{15,16,19–22} aptamers,²³ proteins,^{24–26} nanoparticles^{27,28} and other bioanalytes, by modifying the pore surface^{13,24,29,30} and dimensions.^{18,31} Furthermore, they have been the probe of choice in high-resolution scanning ion conductance microscopy (SICM).^{32,33} Nanopipettes are typically fabricated by laser-assisted pulling, where a glass capillary is exposed to heating and pulling cycle(s), resulting in separation of the capillary into two sharp nanopipettes. Although it is possible to tune the pore dimensions by varying the pulling parameters (temperature, time, pulling strength, *etc.*), pore diameters below 20 nm are generally difficult to achieve. Ideally, significantly smaller nanopore diameters are needed in order to maximise signal-to-noise ratio in nanopore detection. Recently, shrinking of the pore diameter in nanopipettes by electron beam irradiation has been demonstrated,³¹ however, the shrinking process is relatively slow, expensive, and multiple pipettes cannot be processed simultaneously. An alternative approach as proposed in this article is to use atomic layer deposition (ALD), which allows for precise control with angstrom thick resolution to controllably alter the pore dimen-

^aDepartment of Chemistry, Imperial College London, Exhibition Road, South Kensington Campus, London SW7 2AZ, UK.

E-mail: joshua.edel@imperial.ac.uk

^bDepartment of Biomedical Engineering, University of Minnesota, Minneapolis, MN 55455, USA

^cDepartment of Electrical and Computer engineering, University of Minnesota, Minneapolis, MN 55455, USA

† Electronic supplementary information (ESI) available. See DOI: 10.1039/c5an01001b



sions. Importantly, this is a batch process where depositions on multiple pipettes can be performed simultaneously. While ALD has been previously used for controllable shrinking in conventional planar solid-state nanopores,^{34–36} the benefits of ALD have not yet been translated to nanopipette platforms.

Here we show that by depositing Al_2O_3 using ALD it is possible to controllably achieve multiple batches of coated nanopores with dimensions which are sub-10 nm in diameter. This brings the nanopipette dimensions into the same size regime as what is typically used in more conventional solid-state platforms. In addition to controlling nanopore dimensions, ALD functionalization of the nanopipettes allows for modification of the net charge on the nanopore surface. This is particularly useful for quartz and borosilicate glass nanopipettes which have high negative charge compared to conventional planar nanopores. Al_2O_3 has a net positive charge (at $\text{pH} < 9$)³⁷ and ALD can be utilised to modify the interaction between the nanopore and the analyte. Due to ALD's excellent conformal deposition on high aspect ratio structures,^{38–41} both the inner and outer surfaces are coated which is advantageous when interaction between the nanopipette tip and the sample needs to be minimised (*e.g.* in SICM imaging and scanning applications).

Results and discussion

Two classes of quartz pipettes with starting pore diameters of, $d_i = 75 \pm 5$ nm (type i) and $d_{ii} = 25 \pm 3$ nm (type ii), were fabri-

cated by laser-assisted pulling (see the Experimental section for details). This was followed by coating with films of Al_2O_3 using ALD (a schematic is shown in Fig. 1Bii). Al_2O_3 was chosen as the deposition material over other standard gases such as HfO_2 as it has been well-studied and utilized extensively for conformal coating of diverse surfaces^{42–45} as well as its excellent dielectric properties, low capacitance,⁴⁶ good adhesion and high electrical stability. Details on the ALD process are available in the Experimental section, Fig. S1 in the ESI† shows a schematic of the ALD deposition and images of ten pipettes placed inside the ALD chamber. Al_2O_3 was deposited on the pipettes at a rate of 5 Å per min. Al_2O_3 films with thickness of 8, 14 and 17 nm were deposited on the larger pipettes (type i) and layers with thickness of 5 and 8 nm on the smaller pipettes (type ii). For each deposition the Al_2O_3 thickness was confirmed by ellipsometry on silicon substrates adjacent to the nanopipettes. Images of both pipette types, before and after deposition were obtained by scanning electron microscopy (SEM). Fig. 1C shows representative SEM images of a nanopipette with a 25 nm nanopore before deposition and an image of a nanopipette of the same type after 8 nm Al_2O_3 deposition.

ALD coating was further confirmed by ionic current measurements. Ionic transport across the nanopores of both coated and non-coated nanopipette was characterised in 1 M KCl, 10 mM Tris, 1 mM EDTA, pH 8 solution (schematic shown in Fig. 1A). For each nanopipette, multiple chronoamperometric traces (ranging from -500 mV to 500 mV with a 50 mV step) were measured using an Axopatch 200B patch-

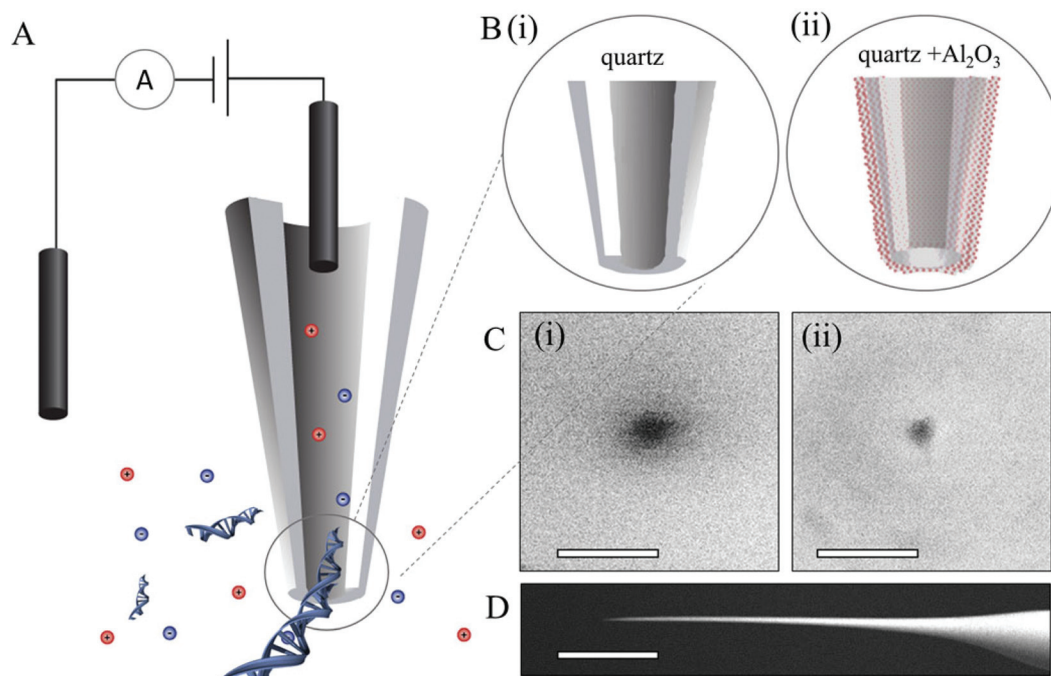


Fig. 1 A. Schematic of the experimental set up with nanopipette. B. Zoomed in schematic of the tip end of the (i) unmodified pipette (ii) Al_2O_3 -ALD-modified pipette. C. SEM characterization of the pore diameter (i) 25 nm and (ii) 7.5 nm. The scale bars are 40 nm. D. SEM image of the nanopipette tip (scale bar is 200 μm).



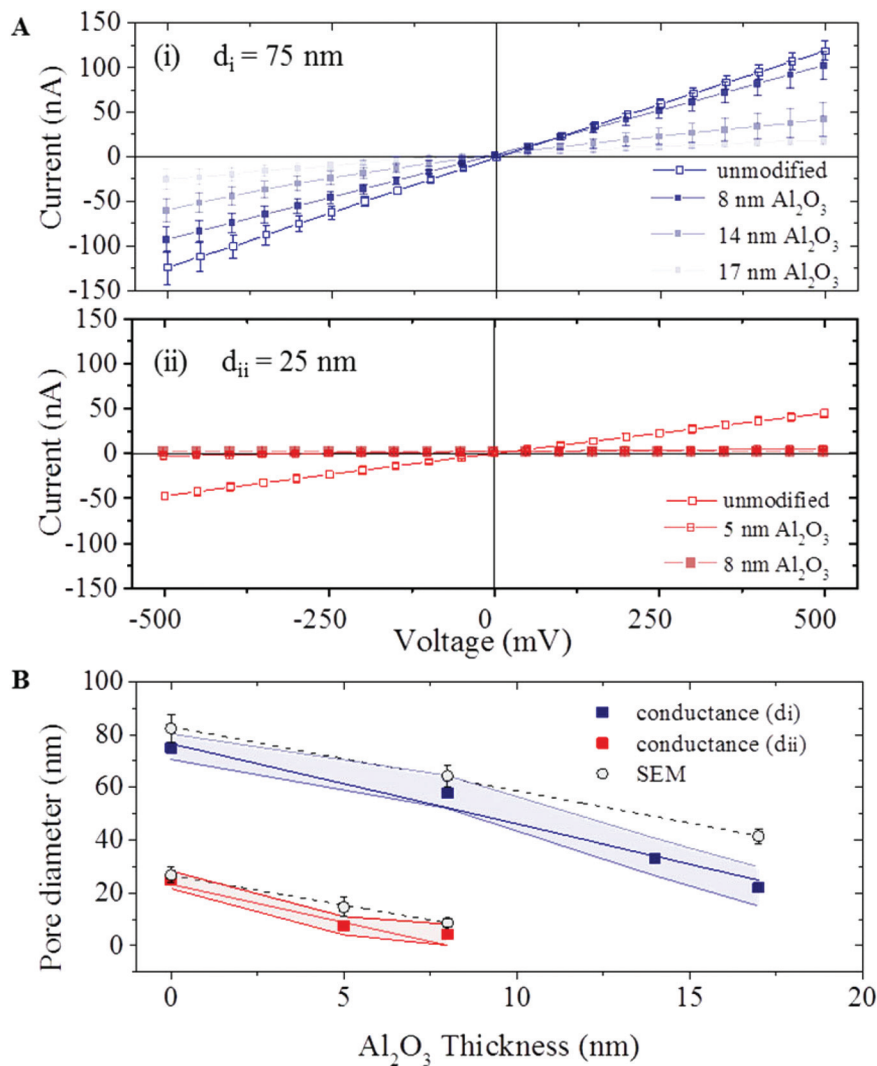


Fig. 2 A (i) $I-V$ characteristics of uncoated and coated (8, 14 and 17 nm Al_2O_3 deposition) pipettes from d_i . (ii) $I-V$ characteristics of uncoated and coated (5 and 8 nm Al_2O_3 deposition) pipettes from d_{ii} . The average $I-V$ curve across the unmodified pipettes was measured with thirty pipettes on both d_i and d_{ii} and all thickness of Al_2O_3 deposition were measured with ten pipettes. The error bars as presented are the standard deviation in the current between individual devices at each voltage from -500 to 500 mV. B The pipette pore diameter is plotted as a function of the thickness of the deposited Al_2O_3 layer, as measured on a planar Si substrate: conductance from type (d_i and d_{ii}) and the average of these devices are shown in (square) and the shaded area (blue and red) represents one standard deviation. The second part which the coated pipette is measured by SEM (circle) (mean value \pm one standard deviation). The diameter of a minimum of ten pipettes at each of the deposition thicknesses of 5, 8, 14 and 17 nm was measured.

clamp amplifier. $I-V$ curves were extracted from the chronoamperometric traces. Fig. 2A shows $I-V$ traces average for 60 pipettes for both types of pipettes before and after the ALD coating. All coated pipettes showed linear $I-V$ (no rectification) indicating no preferential direction for the ion flow. For both nanopipette types the nanopore current (and conductance) systematically decreased with increasing thickness of the Al_2O_3 coating, indicating a decrease in nanopore diameter. To estimate the pore diameter we used the model described by Steinbock *et al.*⁴⁷ (eqn (1), in ESI S2†). Due to the high ionic strength of the solution used (1 M KCl), surface conductivity contributions to the conductance were neglected. For uncoated

pipettes average conductance of 252 ± 16 nS (type i) and 58 ± 5 nS (type ii) were obtained (all error estimates are standard deviations), corresponding to calculated pore diameters of 75 ± 5 nm and 25 ± 3 nm respectively. These values are in agreement with the pore diameters of 82 ± 5 nm and 27 ± 3 nm, measured by SEM imaging. The pore conductance model also provided good agreement between the calculated pore diameter and SEM measurements for ALD coated nanopipettes for both pipette types. Fig. 2B shows plots of pore diameters both calculated from eqn (1), in ESI S2† and from SEM measurements indicating that the diameter of the nanopore decreased linearly with the thickness of deposited Al_2O_3 .



Traditionally, the relationship between Al_2O_3 ALD rate and thickness has been modelled on a flat Si substrate and has been confirmed by *in situ* FTIR^{42,43} and mass spectrometry.⁴⁴ While in Fig. 2B the thickness of the deposited Al_2O_3 was measured on a planar Si substrate, different thicknesses deposited in a pore can be expected due to the different surface chemistry of the pipette and its high-aspect conical geometry. Indeed the rate of shrinking of the nanopore diameters was measurably higher than the rate of deposition on planar Si samples. During the ALD process we expect a 2 nm reduction in the pore diameter with every 1 nm of Al_2O_3 deposition, or conversely, a slope of ~ 2 for the plots presented in Fig. 2B. Instead we measured higher deposition ratios of 3.0 ± 0.3 for type (i) and 2.9 ± 0.8 for type (ii) pipettes. One possible explanation is the change in the reaction conditions inside the nanopipette. The Al_2O_3 ALD growth occurs during alternating exposures to TMA and H_2O . The growth per cycle is dependent on the surface species and surface chemistry.^{42,48,49} During the ALD process, precursor gases are pumped in the chamber sequentially, and react on the surface to form oxide films. Flow through the confined geometry of nanopipette may affect the reaction rate at the surface. In addition, difference in the

surface conditions such as availability of nucleation sites can lead to change in amount of deposited Al_2O_3 .⁵⁰

The ALD coating adds additional dielectric layer, although with higher dielectric constant and dielectric loss factor ($\epsilon = 3.8$ and $D_{\text{loss}} = \sim 10^{-4}$ for quartz and $\epsilon = 9.1$ and $D_{\text{loss}} = \sim 2 \times 10^{-4}$ for Al_2O_3). The non-coated pipettes showed ~ 10 pA root mean square (RMS) current noise at 300 mV, at 10 KHz filtering. The noise performance remained very similar for the coated ALD pipettes with 4.1, 9.8 and 9.7 pA rms current noise, respectively for pipettes coated after 8, 14 and 17 nm Al_2O_3 deposition. Power spectrum density (PSD) plots of these pipettes are presented in ESI S3.†

To demonstrate the functionality and investigate how the deposited Al_2O_3 affects the surface properties of the pipettes, DNA translocation experiments were carried out on ALD-modified nanopores (with diameters of 60 and 7.5 nm). Fig. 3A shows a representative current trace of single-molecule detection of 10 kbp dsDNA with a 7.5 nm pore (similar data for a 60 nm pore are shown in S3A†). The chronoamperometric trace shows characteristic ionic current blockades due to the translocation of the DNA molecules across the pore. Fig. 3B displays an expanded view of 5 representative translocation

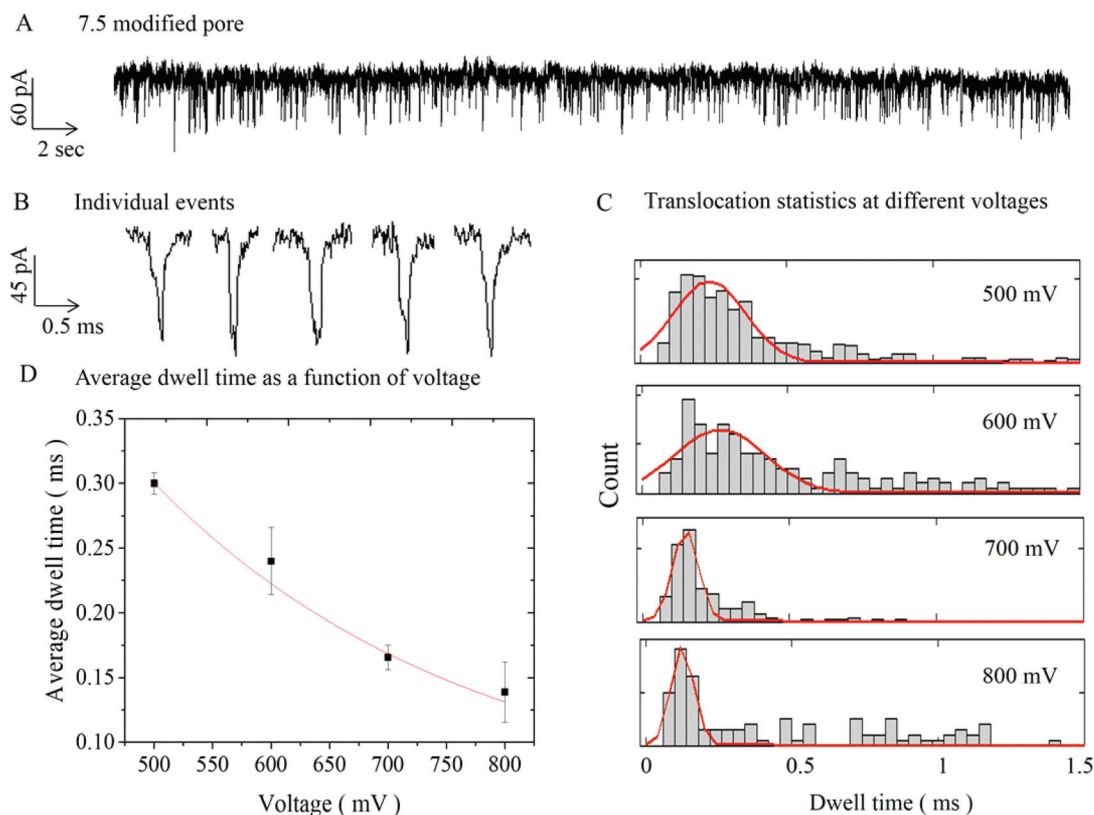


Fig. 3 A Typical current trace on 7.5 nm modified pores after the addition of 100 pM of 10 kbp DNA at 300 mV. Discrete drops in the ion current are clearly observed and corresponding to pore blockades due to the translocation of DNA molecules. B Representative single molecule events on expanded scale. C Histograms of the dwell time distribution for applied voltages from 500–800 mV. D Average dwell time of the modified pore as a function of voltage and the red line showed exponential fit to the data. The average dwell times were 0.30 ± 0.01 , 0.24 ± 0.03 , 0.17 ± 0.01 and 0.14 ± 0.02 ms, respectively, for 500, 600, 700, 800 mV.



events. Additional current traces (for different potentials) and current dwell time scatter plots are available respectively in S4 and S5 in the ESI.†

Experiments of 10 kbp dsDNA translocation through both 60 nm and 7.5 nm diameter pores were performed for range of applied voltage (300–600 mV) and (500–800 mV) respectively, as shown in Fig. 3C and S3C.† The results indicated lower average dwell time with increasing applied voltage. This is as expected, since higher applied voltage results in stronger electrophoretic driving force exerted on the DNA molecules, leading to higher translocation velocities and shorter dwell times.^{39,47,51,52} Fig. 3C shows dwell time histograms at different applied voltages for 7.5 nm pore, (for 60 nm pore data is available in S3C†). Each distribution was fitted with a first-passage probability density function (FP-PDF) as reported by Ling *et al.*⁵³ The FP-PDF is defined by $F(t) = (L/(4\pi Dt^3))^{1/2} e^{-(L - vt)^2/4Dt}$ where D is the diffusion constant, v is the drift velocity, and L is the contour length of the DNA. Slightly longer dwell time and larger peak current were observed with the 7.5 nm pore (0.30 ± 0.01 ms, 122.4 ± 8.9 pA), compared to (0.24 ± 0.02 ms, 95.4 ± 5.6 pA) for the larger 60 nm pore (see S3, ESI†). This can be explained by a stronger DNA–pore interaction in smaller pores.^{54,55} In general, the dwell time and the peak current for 10 kbp DNA were in good agreement with literature values for non-modified solid-state nanopores and nanopipettes.^{2,5,19} The average dwell time for a 7.5 nm pore at 500 mV was 0.30 ± 0.01 ms, which corresponds to a translocation speed of 11.2 ± 0.4 mm s⁻¹. Again, these results are in good agreement with the ones reported by Steinbock *et al.* (10.3 mm s⁻¹),¹⁶ by Li *et al.* (10 mm s⁻¹),⁵ and by Gong *et al.* (8.2 mm s⁻¹).¹⁹ Finally the calculated the excluded ionic charge per translocation event for was 16.9 ± 4.0 fAs and 23.5 ± 12.7 fAs respectively for 60 nm and 7.5 nm pores. These values were found to be in the same order of magnitude as those previously reported in the literature.^{16,19}

For the smaller, 7.5 nm pores, translocation events were observed only for potential above 500 mV. This threshold applied potential required to drive the DNA molecule through the pore, suggests the presence of an entropic barrier. Fig. 3D shows a non-linear decrease of dwell time with increasing voltage, supporting the presence of such barrier during the DNA transport across the pore.^{34,39} In addition for smaller pores, small sub-population events with longer dwell times (>0.5 ms) were observed indicating there is a DNA–modified pore interaction, similar to the effect seen in small solid-state nanopores.⁵⁴

Conclusions

The results confirmed that Al₂O₃ ALD can be used to fine tune nanopipettes to sub 10s nm without interfering with the pore's sensing abilities. The process only requires application of higher electrophoretic force to overcome the entropic barrier and drive the molecules through the narrow nanopores. We also demonstrated that ALD can be used for batch

reduction of nanopipette pore size without any other expensive fabrication facilities. The nanopipettes were fabricated in sub-10s nm and demonstrated good agreement on the translocation times, peak current and excluded ionic charge with results reported for small solid-state nanopores in literature. The modified nanopipettes were characterised using SEM and the images were in good agreement with the electrical data. We also performed voltage dependent translocation studies and showed that translocation times were not affected by the Al₂O₃ modification of pores. Although these modified nanopipettes with reduced pore size offer many advantages, detection using sub-nm pore requires further studies analysing complexities arising due to the confined geometry in the nanopipette. It should be mentioned that ALD is a chemistry driven process hence the deposition result and nanopore performance may vary for difference choice of precursor – substrate systems. Deposition from different precursors would require further investigation, however they can potentially enable modified nanopipette with enhanced surface properties. In the near future, the Al₂O₃ ALD modification can allow detection of smaller molecule sequences or other molecules like RNA to meet the requirements of many different applications and certainly provides a step closer to scale-up in advancing sensing technology.

Methods

Fabrication of nanopipette

A thin glass capillary (Intracel Ltd, UK) length 75 mm with 0.6 mm filament was placed inside the plasma cleaner to ensure all dusts and dirt are removed. After plasma-cleaning, the capillary was placed in a laser-based pipette puller (Sutter Instrument, P-2000). The pipette pulling occurred in two-stage process with stage 1 [Heat:575; Fil:3, Vel:3, Del:145, Pull:75] and pulled a 1.2 mm taper into the capillary before stage 2 [Heat:600; Fil:0, Vel:15, Del:128, Pull:200]. After fabrication, ALD Al₂O₃ was deposited on the nanopipettes. For fabrication of the second batch of pipettes with smaller starting diameter ($d_{ii} = 25 \pm 3$ nm), we used 75 mm long capillary with 0.5 mm filament, followed by plasma-cleaning and placement into the pipette puller. The first pipette pulling stage [Heat:575; Fil:3, Vel:35, Del:145, Pull:75] and pulls a 1.7 mm taper into the capillary before stage 2 [Heat:700; Fil:0, Vel:15, Del:128, Pull:200]. It should be noted that there is some variation between P2000 pullers due to local temperature and humidity therefore these pulling parameters only serve as an example.

ALD deposition

The nanopipettes were further plasma cleaned prior to ALD deposition. The nanopipettes were coated with 5, 8, 14 and 17 nm calculated thickness of alumina (Al₂O₃) using atomic layer deposition (ALD, Savannah, Cambridge Nanotech) at 235 °C. Al₂O₃ has been widely used in the thin film deposition, as the deposited layer is thermally and chemically stable and exhibits negligible ion diffusion. Trimethylaluminium (TMA)



and water vapour were injected sequentially in the chamber with nitrogen (N₂) purging in between the injections. The deposition rate was around 1.1 Å per cycle. Silicon wafers were placed in the chamber along with the nanopipettes and ellipsometry was performed for calibration and checking the thickness of deposited alumina layer.

Solutions and reagents

The buffer solution was made using 1 M KCl, 10 mM Tris and 1 mM EDTA (pH 8). 10 kbp DNA (New England Biolabs) was used for the translocation studies. All DNA samples were diluted to a final concentration of 100 pM in the buffered solution and filtered using a 0.2 µm filter.

Ion current measurement and detection

Ionic current characterisations of the nanopipettes and translocation experiments were carried out with an Axopatch 200B patch clamp current amplifier (Molecular Devices, USA). An Ag/AgCl electrode was inserted into the nanopipette (patch electrode) and in the external reservoir (bath/ground electrode) at positive bias DNA was translocated from the bath towards the interior of the nanopipette. The recorded data was filtered using a 10 kHz, 4-pole Bessel low pass filter. The recorded data was digitized with a Digidata 1440A at 50 kHz was then processed using custom written Matlab code.

Acknowledgements

JBE acknowledges the ERC for a starting investigator grant and the BBSRC for financial support. S.K. and S.-H.O. acknowledge funding from the U.S. National Science Foundation (NSF CAREER Award). This work utilized resources at the University of Minnesota, including the Minnesota Nanofabrication Center, which receives partial support from NSF through the National Nanotechnology Infrastructure Network program.

References

- 1 B. N. Miles, A. P. Ivanov, K. A. Wilson, F. Dogan, D. Japrun and J. B. Edel, *Chem. Soc. Rev.*, 2013, **42**, 15–28.
- 2 C. Dekker, *Nat. Nanotechnol.*, 2007, **2**, 209–215.
- 3 D. G. Haywood, A. Saha-Shah, L. A. Baker and S. C. Jacobson, *Anal. Chem.*, 2015, **87**, 172–187.
- 4 M. J. Kim, M. Wanunu, D. C. Bell and A. Meller, *Adv. Mater.*, 2006, **18**, 3149–3153.
- 5 J. Li, M. Gershow, D. Stein, E. Brandin and J. A. Golovchenko, *Nat. Mater.*, 2003, **2**, 611–615.
- 6 D. S. Jiali Li, C. McMullan, D. Branton, M. J. Aziz and J. A. Golovchenko, *Nature*, 2001, **412**, 166–169.
- 7 J. H. C. A. J. Storm, X. S. Ling, H. W. Zandbergen and C. Dekker, *Nat. Mater.*, 2003, **2**, 537–540.
- 8 H. Chang, F. Kosari, G. Andreadakis, M. Alam, G. Vasmatzis and R. Bashir, *Nano Lett.*, 2004, **4**, 1551–1556.
- 9 G. g. F. Schneider, S. W. Kowalczyk, V. E. Calado, G. g. Pandraud, H. W. Zandbergen, L. M. K. Vandersypen and C. Dekker, *Nano Lett.*, 2010, **10**, 3163–3167.
- 10 C. A. Merchant, K. Healy, M. Wanunu, V. Ray, N. Peterman, J. Bartel, M. D. Fischbein, K. Venta, Z. Luo, A. T. C. Johnson and M. Drndić, *Nano Lett.*, 2010, **10**, 2915–2921.
- 11 J. B. Heng, C. Ho, T. Kim, R. Timp, A. Aksimentiev, Y. V. Grinkova, S. Sligar, K. Schulten and G. Timp, *Biophys. J.*, 2004, **87**, 2905–2911.
- 12 M. Ayub, A. Ivanov, J. Hong, P. Kuhn, E. Instuli, J. B. Edel and T. Albrecht, *J. Phys.: Condens. Matter: an Institute of Physics journal*, 2010, **22**, 454128.
- 13 P. Actis, A. C. Mak and N. Pourmand, *Bioanal. Rev.*, 2010, **1**, 177–185.
- 14 R. A. Levis and J. L. Rae, *Biophys. J.*, 1993, **65**, 1666–1677.
- 15 L. J. Steinbock, R. D. Bulushev, S. Krishnan, C. Raillon and A. Radenovic, *ACS Nano*, 2013, **7**, 11255–11262.
- 16 L. J. Steinbock, O. Otto, C. Chimere, J. Gornall and U. F. Keyser, *Nano Lett.*, 2010, **10**, 2493–2497.
- 17 R. J. White, E. N. Ervin, T. Yang, X. Chen, S. Daniel, P. S. Cremer and H. S. White, *J. Am. Chem. Soc.*, 2007, **129**, 11766–11775.
- 18 N. A. Bell, V. V. Thacker, S. Hernández-Ainsa, M. E. Fuentes-Perez, F. Moreno-Herrero, T. Liedl and U. F. Keyser, *Lab Chip*, 2013, **13**, 1859–1862.
- 19 X. Gong, A. V. Patil, A. P. Ivanov, Q. Kong, T. Gibb, F. Dogan, A. J. deMello and J. B. Edel, *Anal. Chem.*, 2014, **86**, 835–841.
- 20 B. Zhang, M. Wood and H. Lee, *Anal. Chem.*, 2009, **81**, 5541–5548.
- 21 A. P. Ivanov, P. Actis, P. Jönsson, D. Klenerman, Y. Korchev and J. B. Edel, *ACS Nano*, 2015, **9**, 3587–3595.
- 22 T. R. Gibb, A. P. Ivanov, J. B. Edel and T. Albrecht, *Anal. Chem.*, 2014, **86**, 1864–1871.
- 23 P. Actis, A. Rogers, J. Nivala, B. Vilozny, R. A. Seger, O. Jejelowo and N. Pourmand, *Biosens. Bioelectron.*, 2011, **26**, 4503–4507.
- 24 S. Ding, C. Gao and L.-Q. Gu, *Anal. Chem.*, 2009, **81**, 6649–6655.
- 25 W. Li, N. A. W. Bell, S. Hernández-Ainsa, V. V. Thacker, A. M. Thackray, R. Bujdoso and U. F. Keyser, *ACS Nano*, 2013, **7**, 4129–4134.
- 26 L. J. Steinbock, S. Krishnan, R. D. Bulushev, S. Borgeaud, M. Blokesch, L. Feletti and A. Radenovic, *Nanoscale*, 2014, **6**, 14380–14387.
- 27 M. Karhanek, J. T. Kemp, N. Pourmand, R. W. Davis and C. D. Webb, *Nano Lett.*, 2005, **5**, 403–407.
- 28 W.-J. Lan, D. A. Holden, B. Zhang and H. S. White, *Anal. Chem.*, 2011, **83**, 3840–3847.
- 29 S. Umehara, N. Pourmand, C. D. Webb, R. W. Davis, K. Yasuda and M. Karhanek, *Nano Lett.*, 2006, **6**, 2486–2492.
- 30 Y. Fu, H. Tokuhisa and L. A. Baker, *Chem. Commun.*, 2009, 4877–4879.
- 31 L. Steinbock, J. Steinbock and A. Radenovic, *Nano Lett.*, 2013, **13**, 1717–1723.



- 32 P. Novak, C. Li, A. I. Shevchuk, R. Stepanyan, M. Caldwell, S. Hughes, T. G. Smart, J. Gorelik, V. P. Ostanin, M. J. Lab, G. W. J. Moss, G. I. Frolenkov, D. Klenerman and Y. E. Korchev, *Nat. Methods*, 2009, **6**, 279–281.
- 33 A. I. Shevchuk, G. I. Frolenkov, D. Sánchez, P. S. James, N. Freedman, M. J. Lab, R. Jones, D. Klenerman and Y. E. Korchev, *Angew. Chem., Int. Ed.*, 2006, **118**, 2270–2274.
- 34 P. Chen, J. Gu, E. Brandin, Y.-R. Kim, Q. Wang and D. Branton, *Nano Lett.*, 2004, **4**, 2293–2298.
- 35 Y.-R. Kim, J. Min, I.-H. Lee, S. Kim, A.-G. Kim, K. Kim, K. Namkoong and C. Ko, *Biosens. Bioelectron.*, 2007, **22**, 2926–2931.
- 36 B. M. Venkatesan, B. Dorvel, S. Yemenicioglu, N. Watkins, I. Petrov and R. Bashir, *Adv. Mater.*, 2009, **21**, 2771–2776.
- 37 M. Kosmulski, *J. Colloid Interface Sci.*, 2002, **253**, 77–87.
- 38 P. Chen, T. Mitsui, D. B. Farmer, J. Golovchenko, R. G. Gordon and D. Branton, *Nano Lett.*, 2004, **4**, 1333–1337.
- 39 B. M. Venkatesan, A. B. Shah, J.-M. Zuo and R. Bashir, *Adv. Funct. Mater.*, 2010, **20**, 1266–1275.
- 40 B. M. Venkatesan, D. Estrada, S. Banerjee, X. Jin, V. E. Dorgan, M.-H. Bae, N. R. Aluru, E. Pop and R. Bashir, *ACS Nano*, 2012, **6**, 441–450.
- 41 S. M. George, *Chem. Rev.*, 2009, **110**, 111–131.
- 42 A. C. Dillon, A. W. Ott, J. D. Way and S. M. George, *Surf. Sci.*, 1995, **322**, 230–242.
- 43 J. Ferguson, A. Weimer and S. George, *Thin Solid Films*, 2000, **371**, 95–104.
- 44 M. Juppó, A. Rahtu, M. Ritala and M. Leskelä, *Langmuir*, 2000, **16**, 4034–4039.
- 45 M. D. Groner, J. W. Elam, F. H. Fabreguette and S. M. George, *Thin Solid Films*, 2002, **413**, 186–197.
- 46 J. Yota, H. Shen and R. Ramanathan, *J. Vac. Sci. Technol., A*, 2013, **31**, 01A134.
- 47 L. J. Steinbock, A. Lucas, O. Otto and U. F. Keyser, *Electrophoresis*, 2012, **33**, 3480–3487.
- 48 S. M. George, A. W. Ott and J. W. Klaus, *J. Phys. Chem.*, 1996, **100**, 13121–13131.
- 49 A. W. Ott, J. W. Klaus, J. M. Johnson and S. M. George, *Thin Solid Films*, 1997, **292**, 135–144.
- 50 C. A. Wilson, R. K. Grubbs and S. M. George, *Chem. Mater.*, 2005, **17**, 5625–5634.
- 51 A. Meller, L. Nivon and D. Branton, *Phys. Rev. Lett.*, 2001, **86**, 3435–3438.
- 52 S. W. Kowalczyk, M. W. Tuijtel, S. P. Donkers and C. Dekker, *Nano Lett.*, 2010, **10**, 1414–1420.
- 53 D. Y. Ling and X. S. Ling, *J. Phys.: Condens. Matter: an Institute of Phys. J.*, 2013, **25**, 375102.
- 54 S. Carson, J. Wilson, A. Aksimentiev and M. Wanunu, *Biophys. J.*, 2014, **107**, 2381–2393.
- 55 R. Akahori, T. Haga, T. Hatano, I. Yanagi, T. Ohura, H. Hamamura, T. Iwasaki, T. Yokoi and T. Anazawa, *Nanotechnology*, 2014, **25**, 275501.

